Dielectric and transport properties of a supercooled symmetrical molten salt

S. D. Wilke, H. C. Chen, and J. Bosse*
Institut für Theoretische Physik, Freie Universität Berlin, Arnimallee 14, D-14195 Berlin, Germany
(Received 12 February 1999; revised manuscript received 4 June 1999)

The liquid-glass transition of the restricted primitive model for a symmetrical molten salt is studied using mode-coupling theory. The transition at high densities is predicted to obey the Lindemann criterion for melting, and the charge-density peak found in neutron-scattering experiments on ionic glass formers is qualitatively reproduced. Frequency-dependent dielectric functions, shear viscosities, and dynamical conductivities of the supercooled liquid are presented. Comparing the latter to the diffusion constant, we find that mode-coupling theory reproduces the Nernst-Einstein relation. The Stokes-Einstein radius is found to be approximately equal to the particle radius only near the high-density glass transition. [S1063-651X(99)08609-2]

PACS number(s): 64.70.Pf, 66.10.−x, 66.20.+d

I. INTRODUCTION

Ionic glasses have potentially important technological applications, for example, as glassy ionic conductors in solid-state batteries. However, there has been only slow progress in the theoretical understanding of these systems and their properties so far. Two major difficulties have impeded the investigation of ionic glasses: First, glasses in general are systems far from thermodynamic equilibrium and, therefore, generally require sophisticated concepts of statistical mechanics. In addition, ionic systems in particular cause further theoretical complications since they contain two or more different particle species.

A breakthrough concerning the first problem was the application of mode-coupling theory (MCT) to the liquid-glass transition [1,2]. Explaining the transition as induced by nonlinear feedback processes, MCT has led to considerable progress in the research on glasses formed from simple fragile liquids (see, e.g., Ref. [3]). Soon after the pioneering papers of MCT were published, the theory was extended to multicomponent (including ionic) systems. The first ionic liquid discussed within the framework of MCT was a system of oppositely charged, but otherwise identical particles— the so-called symmetrical molten salt (SMS) [4–7]. However, the discussion was carried out using only a ''schematic model'' of the SMS, which could not be expected to describe realistic systems in much detail since it neglected spatial variations of density correlations by restricting to a single wave number. Despite this drastic simplification, the schematic model exhibited some interesting features and triggered new experimental and theoretical research [8,9].

Here we present a new MCT study of the SMS, which, in contrast to the earlier investigations, includes the complete wave-number dependence, allowing for a realistic account of the SMS glass transition as a prototype of the glassification of ionic melts in general. A preceding analysis of the low-density regime with this method has recently predicted a ''Wigner'' glass phase of the SMS [10], similar to the one observed experimentally in colloidal [11] and plasma [12] systems. In this paper, we concentrate on typical liquid densities and demonstrate the large scope of experimentally relevant information that can be extracted from MCT. We have put special emphasis on the characteristic change of transport coefficients like conductivity, shear viscosity, and diffusion constant, in the vicinity of the transition. In particular, we derive predictions on the validity of the Nernst-Einstein relation and obtain an effective particle radius from the Stokes-Einstein relation. These are especially interesting points because there are contradictory results in literature [13–15].

The paper is organized as follows: Following this introduction, we give a sketch of MCT for the SMS and of the description of its dielectric and conductor properties in Sec. II. Our results are divided into two major parts, Sec. III on the static properties obtained from the long-time limit, and Sec. IV, which contains a discussion of time-dependent quantities. In Sec. V, we summarize and make some concluding remarks. Three rather technical paragraphs are included as appendices.

II. FORMAL FRAMEWORK

A. Mode-coupling theory of the SMS

The central concept of MCT is the (classical) Kubo relaxation function defined by

$$\Phi_{AB}(t) := \beta \langle \delta A^{\dagger}(t)\, \delta B \rangle = (A | \mathrm{e}^{-\mathrm{i}\mathcal{L}t} | B) \tag{1}$$

for two dynamical variables A and B, where $\langle \ldots \rangle$ denotes a thermal equilibrium average, $\delta A := A - \langle A \rangle$ and $\beta := 1/(k_{\mathrm{B}}T)$. To simplify the notation, we have introduced Mori's scalar product $(A|B) := \beta \langle \delta A^{\dagger} \delta B \rangle$ in the vector space of dynamical variables [16], and the generator of time propagation, the Liouvillian $\mathcal{L} := \mathrm{i}\{H, \cdot\}$. The thermodynamic limit is to be taken at the end of the calculations.

We will consider a classical SMS, i.e., a two-component system of oppositely charged, but otherwise identical particles. In addition to homogeneity, isotropy and time-inversion symmetry, which are generally assumed for liquids, the SMS is invariant under charge conjugation. To exploit this symmetry, we choose a description in terms of mass- and charge-density variables, $M(\mathbf{q}) := \sqrt{n/2}[N^{(1)}(\mathbf{q}) + N^{(2)}(\mathbf{q})]$ and $C(\mathbf{q}) := \sqrt{n/2}[N^{(1)}(\mathbf{q}) - N^{(2)}(\mathbf{q})]$, resp., where $n = N/V$ is the mean-particle density. The variable

*Author to whom correspondence should be addressed.

$N^{(s)}(\mathbf{q}) := \Sigma_{j=1}^{N/2} \exp[-i\mathbf{q}\cdot\mathbf{r}_j^{(s)}]/\sqrt{N/2}$ is the number density of species s. We will be concerned with the Kubo relaxation functions of mass and charge, $\Phi_M(q;t) := \Phi_{M(\mathbf{q})M(\mathbf{q})}(t)$ and $\Phi_C(q;t) := \Phi_{C(\mathbf{q})C(\mathbf{q})}(t)$, respectively. Obviously, charge-conjugation symmetry implies $\Phi_{M(\mathbf{q})C(\mathbf{q})}(t) \equiv 0$.

Two formally exact equations of motion for these relaxation functions can be derived by employing the Mori-Zwanzig formalism [16,17]. It can be applied either to the variables $N^{(1)}(\mathbf{q})$ and $N^{(2)}(\mathbf{q})$, followed by a transformation of the relaxation functions as described in Appendix B, or directly to $M(\mathbf{q})$ and $C(\mathbf{q})$. Either approach results in the same two generalized-oscillator equations of motion, the Fourier-Laplace transforms (defined by $f(z) := i\int_0^\infty dt \exp(itz) f(t)$ for a function f) of which read

$$\Phi_\sigma(q,z) = -\Phi_\sigma(q;t=0)\left[z - \frac{\Omega_\sigma^2(q)}{z + K_\sigma(q,z)}\right]^{-1}, \qquad \sigma \in \{M,C\} \tag{2}$$

The initial conditions for the relaxation functions are determined by the mass- and charge-structure factors

$$\Phi_M(q;t=0) = \beta n S_M(q) \overset{q\to 0}{\to} n^2 \kappa_T, \tag{3}$$

$$\Phi_C(q;t=0) = \beta n S_C(q) \overset{q\to 0}{\to} \epsilon_0 q^2/(Ze)^2, \tag{4}$$

which, in turn, are obtained from the partial-density static structure factors via $S_M(q) := S_{11}(q) + S_{12}(q)$ and $S_C(q) := S_{11}(q) - S_{12}(q)$ in the case of the SMS. Ze denotes the magnitude of charge of an individual particle, and κ_T is the system's isothermal compressibility. The characteristic frequencies $\Omega_M^2(q)$ and $\Omega_C^2(q)$ can also be expressed in terms of the static structure,

$$\Omega_M^2(q) := \frac{q^2 v_{\rm th}^2}{S_M(q)} \overset{q\to 0}{\to} \frac{q^2}{mn\kappa_T}, \tag{5}$$

$$\Omega_C^2(q) := \frac{q^2 v_{\rm th}^2}{S_C(q)} \overset{q\to 0}{\to} \omega_{\rm pl}^2, \tag{6}$$

with the particle mass m, the thermal particle velocity $v_{\rm th} := (\beta m)^{-1/2}$, and the plasma frequency $\omega_{\rm pl}^2 := (Ze)^2 n/(\epsilon_0 m)$. Within MCT, the relaxation kernels $K_M(q,z)$ and $K_C(q,z)$ are written as the sum of a regular and a mode-coupling contribution,

$$K_\sigma(q,z) = K_\sigma^{\rm reg}(q,z) + K_\sigma^{\rm MC}(q,z), \qquad \sigma \in \{M,C\} \tag{7}$$

The regular contributions approach finite limits for $z \to 0$, whereas the mode-coupling parts may show a small-frequency singularity. The mode-coupling approximation (MCA), a derivation of which is given in Appendix A, leads to expressions for $K_M^{\rm MC}(q,z)$ and $K_C^{\rm MC}(q,z)$ in terms of the relaxation functions and the static structure,

$$K_M^{\rm MC}(q;t) = \frac{v_{\rm th}^2}{8\beta^2 n}\frac{1}{V}\sum_{\mathbf{k}}\sum_{\sigma\mu}\delta_{\sigma\mu}[k_\parallel c_\sigma(k) + p_\parallel c_\mu(p)]^2 \Phi_\sigma(k;t)\Phi_\mu(p;t) \tag{8}$$

$$K_C^{\rm MC}(q;t) = \frac{v_{\rm th}^2}{8\beta^2 n}\frac{1}{V}\sum_{\mathbf{k}}\sum_{\sigma\mu}(1-\delta_{\sigma\mu})[k_\parallel c_\sigma(k) + p_\parallel c_\mu(p)]^2 \Phi_\sigma(k;t)\Phi_\mu(p;t), \tag{9}$$

where σ and μ take on the indices M and C, and $\mathbf{p}$ abbreviates $\mathbf{q}-\mathbf{k}$. The transformed direct correlation functions $c_M(q) := c_{11}(q) + c_{12}(q)$ and $c_C(q) := c_{11}(q) - c_{12}(q)$, and the notation $k_\parallel := \mathbf{k}\cdot\mathbf{q}/q$ have been introduced. Note that the charge-density relaxation kernel exclusively contains cross products of the form $\Phi_M\Phi_C$, while $\Phi_M\Phi_M$ and $\Phi_C\Phi_C$ only appear in the mass-density relaxation kernel. This observation was the basis of the schematic model for the SMS [4].

Assuming the static structure to be known and the regular part of the memory kernel to be negligible for long times near the glass transition, MCA's (7)–(9) close equations of motion (2) and give rise to a pair of coupled nonlinear integro-differential equations to be solved for $\Phi_M(q;t)$ and $\Phi_C(q;t)$.

Formally, the two equations of motion (2) can be combined into one by including the index for mass and charge in an ''extended'' wave-vector index, $\hat{q} := (q,\mu)$, $\mu \in \{M,C\}$. With these extended wave vectors, the equations of motion take on the form of a one-component theory discussed in Ref. [2]. A glance at relaxation kernels (8) and (9) shows that the vertex functions are non-negative and symmetric with respect to the exchange $(k,\sigma) \leftrightarrow (p,\mu)$. These properties guarantee that the analytical results from the one-component MCT [18] remain valid for the two-component SMS.

In view of later calculations, it is convenient to introduce normalized relaxation functions via

$$\phi_\sigma(q;t) := \frac{\Phi_\sigma(q;t)}{\Phi_\sigma(q;t=0)}, \qquad \sigma \in \{M,C\} \tag{10}$$

The long-time limits of these normalized functions, $f_\sigma(q) := \lim_{t\to\infty}\phi_\sigma(q;t)$ for $\sigma \in \{M,C\}$, vanish identically in the liquid phase, while they are nonzero in the glass phase. They are consequently referred to as nonergodicity parameters (NEPs). A necessary condition for the NEPs can be obtained by multiplying Eq. (2) with $-z$ and taking the limit $z \to i0$:

$$\frac{f_\sigma(q)}{1-f_\sigma(q)} = \frac{K_\sigma^{\rm MC}(q;t=\infty)}{\Omega_\sigma^2(q)}, \qquad \sigma \in \{M,C\} \tag{11}$$

Equation (11), together with MCA relaxation kernels (8) and (9), are two coupled nonlinear integral equations, which enable the calculation of the nonergodicity parameters $f_M(q)$ and $f_C(q)$.

Occasionally, we will use the relaxation functions $\Phi_{ss'}(q;t) := \Phi_{N^{(s)}(\mathbf{q})N^{(s')}(\mathbf{q})}(t)$ of the number densities $N^{(s)}(\mathbf{q})$. These relaxation functions can be obtained from $\Phi_C(q;t)$ and $\Phi_M(q;t)$ by linear combination,

$$\Phi_{ss'}(q;t)=\frac{1}{2n}[\Phi_M(q;t)+(-1)^{s+s'}\Phi_C(q;t)], \quad (12)$$

see Appendix B. Conventionally, they are normalized by [19]

$$\phi_{ss'}(q;t):=\frac{\Phi_{ss'}(q;t)}{\sqrt{\Phi_{ss}(q;t=0)\Phi_{s's'}(q;t=0)}}, \quad (13)$$

and the diagonal elements ($s=s'$) of the long-time limits $f_{ss'}(q):=\lim_{t\to\infty}\phi_{ss'}(q;t)$ are referred to as Debye-Waller factors.

The relaxation function of the number density of a single additional ''tagged'' particle of species $s=1$ or $s=2$, $\Phi_s(q;t):=\Phi_{N_0^{(s)}(\mathbf{q})N_0^{(s)}(\mathbf{q})}(t)$, with $N_0^{(s)}(\mathbf{q}):=\exp[-i\mathbf{q}\mathbf{r}_0^{(s)}]$, can also be calculated within the framework of MCT. One finds that it is given by an expression analogous to Eq. (2),

$$\Phi_s(q,z)=-\beta\left[z-\frac{q^2v_{\rm th}^2}{z+K_s(q,z)}\right]^{-1}. \quad (14)$$

The memory kernel is again split up into $K_s(q,z)=K_s^{\rm reg}(q,z)+K_s^{\rm MC}(q,z)$, and the MCA yields [19]

$$K_s^{\rm MC}(q;t)=\frac{nv_{\rm th}^2}{2\beta^2}\frac{1}{V}\sum_{\mathbf{k}}k_\parallel^2 \times\sum_{\sigma,\sigma'=1}^{2}c_{\sigma s}(k)\Phi_{\sigma\sigma'}(k;t)c_{\sigma' s}(k)\Phi_s(p;t) \quad (15)$$

for the mode-coupling contribution, which dominates $K_s(q;t)$ at long times. Again we have set $\mathbf{p}:=\mathbf{q}-\mathbf{k}$. The long-time limits $f_s(q):=\beta^{-1}\lim_{t\to\infty}\Phi_s(q;t)$ of the (normalized) incoherent relaxation functions are the Lamb-Mößbauer factors.

The transversal mass-current density relaxation kernel, which determines the shear viscosity of the liquid, is obtained by transforming Eq. (34) of Ref. [20] into mass/charge-variable form. One finds

$$K_\perp^{\rm MC}(q;t)=\frac{v_{\rm th}^2}{8\beta^2 n}\frac{1}{V}\sum_{\mathbf{k}}\sum_{\sigma\mu}\delta_{\sigma\mu}[k_\perp c_\sigma(k)-p_\perp c_\mu(p)]^2\Phi_\sigma(k;t)\Phi_\mu(p;t) \quad (16)$$

within MCT. Note the similarity to the longitudinal kernel Eq. (9), and that no further approximations were necessary.

B. Description of dielectric properties

The (longitudinal) dielectric function $\epsilon(q,\omega)$ and the conductivity $\sigma(q,\omega)$ are among the generalized transport coefficients that can be calculated once the density-relaxation functions of the system are known. For any isotropic and homogeneous system of charged particles one has [21]

$$\epsilon(q,\omega)\equiv 1+i\frac{\sigma(q,\omega)}{\epsilon_0\omega}=\frac{1}{1-\dfrac{\Phi_C(q;t=0)}{\epsilon_0q^2/(Ze)^2}[1+\omega\phi_C(q,\omega+i0)]}. \quad (17)$$

We note that a conductor-insulator transition is expected to be associated with the liquid-glass transition of the SMS since the charge-carrying particles become localized. Near the transition, both conductivity and permittivity will exhibit a behavior qualitatively different from that known for simple Drude conductors or the well-known Debye dielectrics. In order to appreciate the results derived from MCT, it is useful to have in mind a simple model of the charge-current relaxation kernel $K_C(q;t)$, which will reduce to the well-known textbook models (Drude, Debye) in limiting cases. For this purpose, we rewrite Eq. (17) by inserting the generalized-oscillator equation of motion (2). We will make use of the f-sum rule, which takes on the form $\Omega_C^2(q)\Phi_C(q;0)=\epsilon_0q^2\omega_{\rm pl}^2/(Ze)^2$ here, and introduce three abbreviations: The normalized (reduced) current relaxation kernel,

$$\tilde{k}(q;t):=\frac{K_C(q;t)-K_C(q;\infty)}{K_C(q;0)-K_C(q;\infty)} \quad (18)$$

as well as its Fourier-Laplace transform $\tilde{k}(q,z)$, the static dielectric function

$$\epsilon_{\rm st}(q):=\lim_{\omega\to0}\epsilon(q,\omega)=\frac{1}{1-\dfrac{\Phi_C(q;0)}{\epsilon_0q^2/(Ze)^2}[1-f_C(q)]} \quad (19)$$

$$=1+\frac{\omega_{\rm pl}^2}{\Omega_C^2(q)-\omega_{\rm pl}^2+K_C(q;\infty)}$$

$$\overset{q\to0}{\to}\ 1+\frac{\omega_{\rm pl}^2}{K_C(t=\infty)}=:\epsilon_{\rm st}, \quad (20)$$

and its high-frequency analogue

$$\epsilon_\infty(q):=1+\frac{\omega_{\rm pl}^2}{\Omega_C^2(q)-\omega_{\rm pl}^2+K_C(q;0)}\overset{q\to0}{\to}1+\frac{\omega_{\rm pl}^2}{K_C(t=0)}=:\epsilon_\infty. \quad (21)$$

A theoretical determination of the latter quantity requires knowledge of the total spectral weight $K_C(q;0)=2/\pi\int_0^\infty d\,\omega K_C''(q,\omega)$. If the spectrum $K_C''(q,\omega):=\mathrm{Im}[K(q,\omega+i0)]$ has its weight at very low frequencies $\omega<\omega_{\rm max}\ll\omega_\infty\ll\omega_{\rm pl}$ only, i.e. if $K_C''(q,\omega)\approx0$ for $\omega>\omega_{\rm max}$, the above quantity will be measurable as the ''high-frequency dielectric constant,'' $\epsilon_\infty(q)=\epsilon(q,\omega_\infty)$.

From equation of motion (2) together with Eqs. (17)–(21) one finds for the response to a homogeneous ($q\to0$) external field of frequency ω,

$$\epsilon(\omega)\equiv 1+\mathrm{i}\frac{\sigma(\omega)}{\epsilon_0\omega}$$
$$=1-\omega_{\mathrm{pl}}^2\left\{\omega^2-\frac{\omega_{\mathrm{pl}}^2}{\epsilon_{\mathrm{st}}-1}+\frac{\omega_{\mathrm{pl}}^2[\epsilon_{\mathrm{st}}-\epsilon_\infty]}{[\epsilon_{\mathrm{st}}-1][\epsilon_\infty-1]}\omega\tilde{k}(\omega+\mathrm{i}0)\right\}^{-1}. \quad (22)$$

Note that we indicate the $(q=0)$ limit of a function by simply omitting the variable q in the list of arguments. The form of Eq. (22) will remain valid for all $q>0$.

A very simple model for the charge-current relaxation kernel $K_C(t)$ is the sum of a slowly decaying contribution of relative weight $\tilde{f}<1$ (relaxation time τ_1) and a quickly decaying contribution of relative weight $[1-\tilde{f}]$ (relaxation time τ_2):

$$K_C(t)\approx K_C(t=0)[\tilde{f}e^{-|t|/\tau_1}+(1-\tilde{f})e^{-|t|/\tau_2}]. \quad (23)$$

For *finite* relaxation times $(\infty>\tau_1>\tau_2>0)$, this Ansatz will model a *conductor*. The relaxation kernel will vanish for $t\to\infty$ resulting in a divergent dielectric constant $\epsilon_{\mathrm{st}}=\infty$ and a finite dc-conductivity

$$\sigma_0=\epsilon_0\omega_{\mathrm{pl}}^2\{K_C(t=0)[\tilde{f}\tau_1+(1-\tilde{f})\tau_2]\}^{-1}. \quad (24)$$

While for $\tilde{f}=0$ and a short relaxation time $(\omega_{\mathrm{pl}}\tau_2\ll 1)$ the above Ansatz describes a Drude conductor to a good approximation,

$$\sigma(\omega)\approx\sigma(\omega)^{\mathrm{Drude}}:=\frac{\sigma_0}{1-\mathrm{i}\omega\tau} \quad (25)$$

with $\tau:=[K_C''(\omega=0)]^{-1}=[K_C(t=0)\tau_2]^{-1}$; strong deviations from Drude behavior can be achieved for $\tilde{f}>0$ and large relaxation times τ_1 and τ_2. In particular, the dc conductivity will vanish like $\sigma_0\propto\tau_1^{-1}$ if the larger relaxation time is increased to $\omega_{\mathrm{pl}}\tau_1\gg 1$. This gives a crude description of what is to be expected when the system is approaching the glass transition. The transformation to a glass associated with a conductor-insulator transition of the model will be completed when $\tau_1=\infty$. According to Eq. (24) then $\sigma_0=0$, and a finite dielectric constant ϵ_{st} is implied by $K_C(t=\infty)=\tilde{f}K_C(t=0)>0$. In this case the normalized relaxation kernel corresponding to Eq. (23) reduces to the simple Debye form

$$\tilde{k}(t)=\exp(-|t|/\tau_2)\Leftrightarrow\omega\tilde{k}(\omega+\mathrm{i}0)=\frac{1}{1-\mathrm{i}\omega\tau_2}-1, \quad (26)$$

and it is straightforward to show that, for sufficiently small frequencies $(\omega\ll\omega_{\mathrm{pl}})$ and large relaxation times $(\omega_{\mathrm{pl}}\tau_2\gg 1)$, Eq. (22) will reduce to the well-known Debye form

$$\epsilon(\omega)\approx\epsilon(\omega)^{\mathrm{Debye}}:=\epsilon_\infty+(\epsilon_{\mathrm{st}}-\epsilon_\infty)\frac{1}{1-\mathrm{i}\omega\tau_{\mathrm{D}}} \quad (27)$$

with the Debye relaxation time $\tau_{\mathrm{D}}:=\tau_2(\epsilon_{\mathrm{st}}-1)/(\epsilon_\infty-1)$.

It is well known that the simple Ansatz, Eq. (23), usually fails to describe $\epsilon(\omega)$ and $\sigma(\omega)$ for supercooled liquids. These systems exhibit very slow nonexponential decay of $\tilde{k}(t)$. Much better fits to the relaxation behavior of a supercooled liquid can be achieved with a modified Ansatz [22],

$$\omega\tilde{k}(\omega+\mathrm{i}0)=\tilde{f}\left[\frac{1}{(1-\mathrm{i}\omega\tau_1)^{\beta_1}}-1\right]+(1-\tilde{f})\times\left[\frac{1}{1+(-\mathrm{i}\omega\tau_2)^{\beta_\omega}}-1\right] \quad (28)$$

and $\epsilon_{\mathrm{st}}=\infty$, corresponding to an extremely slowly decaying contribution of the Cole-Davidson type $(\tau_1\gg\tau_2$ and $0<\beta_1<1)$ and a faster relaxing term of the Cole-Cole type $(\omega_{\mathrm{pl}}\tau_2\gg 1$ and $0<\beta_\omega\leqslant 1)$. Here the Cole-Cole exponent β_2 has been replaced by the frequency-dependent exponent $\beta_\omega:=\beta_2+(1-\beta_2)/(1+\omega^2\tau_{\mathrm{s}}^2)$, in order to guarantee the correct analytical behavior of the relaxation kernel in the limit $\omega\to 0$. To avoid a disturbance of the β relaxation, $\tau_{\mathrm{s}}\gg\tau_2$ must be chosen; we found $\tau_{\mathrm{s}}=10^3\sqrt{\tau_1\tau_2}$ to be reasonable.

The model Eq. (28) results in a dielectric function, the real part of which exhibits three different plateaus (when plotted versus $\log_{10}[\omega]$),

$$\mathrm{Re}[\epsilon(\omega)]\approx\begin{cases}\epsilon^{\mathrm{I}} & \text{for} \quad \omega_{\mathrm{pl}}\gg\omega\gg\tau_2^{-1}\gg\tau_1^{-1}\\ \epsilon^{\mathrm{II}} & \text{for} \quad \omega_{\mathrm{pl}}\gg\tau_2^{-1}\gg\omega\gg\tau_1^{-1}\\ \epsilon^{\mathrm{III}} & \text{for} \quad \omega_{\mathrm{pl}}\gg\tau_2^{-1}\gg\tau_1^{-1}\gg\omega.\end{cases} \quad (29)$$

While in the high-frequency region one recovers $\epsilon^{\mathrm{I}}\approx\epsilon_\infty$ as expected from the discussion following Eq. (21); one finds a larger value

$$\epsilon^{\mathrm{II}}=\epsilon_{\mathrm{st}}^{\mathrm{c}}:=\epsilon_\infty+(\epsilon_\infty-1)\frac{1-\tilde{f}}{\tilde{f}} \quad (30)$$

for intermediate frequencies. The height of this plateau can be identified with the dielectric constant $\epsilon_{\mathrm{st}}^{\mathrm{c}}\equiv\epsilon(\omega=0)$ expected at the transition, since the insulator condition $\tau_1=\infty$ in this case extends the intermediate region down to $\omega=0$ suppressing the formation of a third plateau. This implies that, at the transition point, the second plateau extends out to $\ln\omega=-\infty$ and its value is the critical dielectric constant. As long as $\tau_1<\infty$, however, an even larger plateau is created by the limiting value

$$\epsilon^{\mathrm{III}}=\lim_{\omega\to 0}\mathrm{Re}[\epsilon(\omega)]=\epsilon_{\mathrm{st}}^{\mathrm{c}}+(\epsilon_{\mathrm{st}}^{\mathrm{c}}-1)\frac{1-\beta_1}{2\beta_1} \quad (31)$$

for very low frequencies $(\omega\tau_1\ll 1)$ as long as $\beta_1<1$. The value of ϵ^{III} follows from the low-frequency expansion of the model Eq. (28),

$$\epsilon(\omega)=\mathrm{i}\frac{\sigma_0}{\epsilon_0\omega}+\epsilon^{\mathrm{cond}}+\mathcal{O}((\omega_{\mathrm{pl}}\tau_{\mathrm{s}})^2(\omega\tau_1)\ln[\omega\tau_1];\omega\tau_1) \quad (32)$$

with the dc conductivity $\sigma_0\rightsquigarrow\epsilon_0(\epsilon_{\mathrm{st}}^{\mathrm{c}}-1)/(\beta_1\tau_1)$ and the limiting value $\epsilon^{\mathrm{cond}}=\lim_{\omega\to 0}\mathrm{Re}[\epsilon(\omega)]\rightsquigarrow(\epsilon_{\mathrm{st}}^{\mathrm{c}}+1)/2+(\epsilon_{\mathrm{st}}^{\mathrm{c}}$

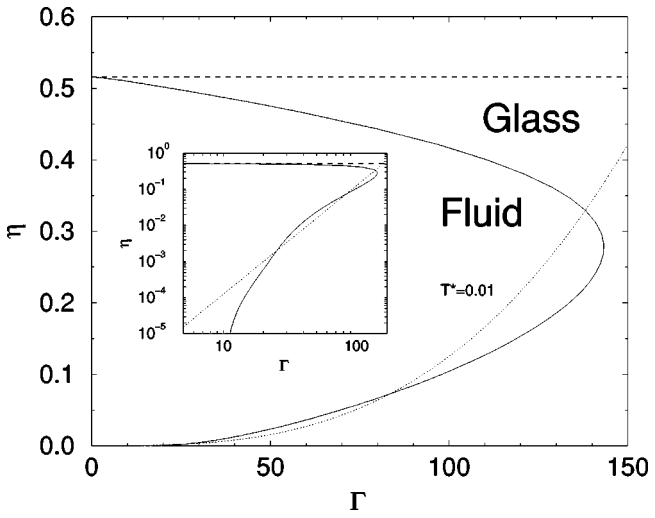

FIG. 1. Fluid-glass phase diagram of the RPM (solid line) and of neutral hard spheres (dashed line). Dotted line: $\eta(\Gamma)$ at constant temperature $T^*=0.01$. Inset: Same curves in a log-log plot.

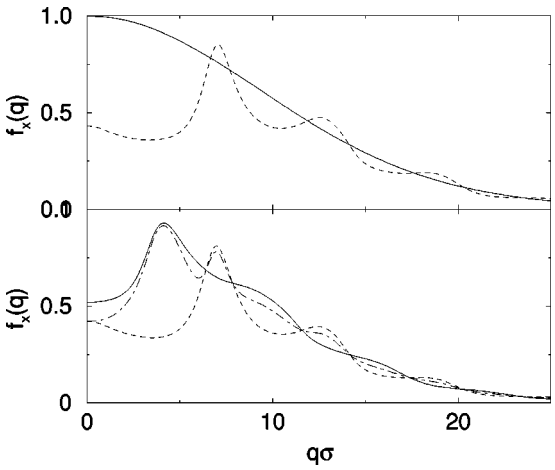

FIG. 2. Critical NEPs of the RPM. Upper panel: $f_C(q)$ (solid line) and $f_M(q)$ (dashed line) at ($\eta\approx0.513$, $T^*\approx0.312$). Lower panel: $f_C(q)$ (solid line), $f_M(q)$ (dashed line), and $f_{11}(q)$ (dot-dashed line) at ($\eta\approx0.0327$, $T^*\approx0.0111$).

$-1)/(2\beta_1)$, from which it can also be seen that the dielectric constant of the supercooled liquid has a diverging imaginary part, while the real part approaches a finite limit.

The model Eq. (28) will be compared to the MCT result in Sec. IV D.

III. STATIC PROPERTIES

We have chosen to study the restricted primitive model (RPM) of an SMS, a model in which the particles are assumed to be hard spheres with diameter σ. Using the iteration procedure described in Ref. [23], the MCT equations of the RPM for the long-time limits $f_{ss'}(q)$ were solved numerically on a mesh of 301 wave numbers. The input static structure factors were taken from mean-spherical approximation (MSA) calculations [24]. The corresponding NEPs for the mass and charge density were then obtained from inverting Eq. (12). To check our calculations, we also solved Eq. (11) for the mass and charge density NEPs directly using the static mass- and charge-structure factors given explicitly in Appendix C, which yielded the same results, as expected.

A. Fluid-glass phase diagram

The liquid-glass phase diagram [10] obtained from the NEPs is presented in Fig. 1 as a plot of the critical packing fraction $\eta_c:=\pi n\sigma^3/6$ as a function of the plasma parameter $\Gamma:=2\sqrt[3]{\eta}/T^*$, where $T^*:=k_BT4\pi\epsilon_0\sigma/(Ze)^2$ is a rescaled temperature. (The (critical) packing fraction η (η_c) introduced here must not be confused with the shear viscosity, η_s, used in Secs. IV C and IV G.) For high temperatures or weak coupling ($\Gamma\to0$), the critical density approaches the limiting value $\eta_c\approx0.516$ known from neutral hard-sphere systems. At lower temperatures, e.g., at $T^*\approx0.01$, we find a reentrant phenomenon in the phase diagram: By isothermal expansion, the high-density glass at $\eta\approx0.5$ first melts as expected. At some intermediate density, there is a *reentrance* into the glassy state. As the density is decreased even more, the glass finally melts again and remains in the fluid phase for all lower densities, as can be seen from the log-log plot of the phase diagram shown in the inset of Fig. 1. Similar reentrant phenomena have been found in a theoretical mode-coupling study of *screened* charged hard spheres [25] provided that the screening length was chosen sufficiently large, and in a theoretical investigation on macroionic suspensions [26]. It was suggested that the second melting of the macroionic suspension could be caused by a strong screening of charges, leaving only rather weak interactions between particles. In that work, the reentrant phenomenon was found in a phase diagram calculated solely from the structure factor. The explanation in terms of such *static* screening properties of the system is definitely *not* valid in the present study, where the reentrant phase-transition line appears to be independent of the peaks in the underlying static structure factor. This indicates the relevance of *dynamical* processes for an explanation of the SMS reentrant behavior.

In the limit of very low densities, MCT predicts a structural arrest of the fluid if temperature is sufficiently low [10]. This effect relies on the long range of Coulomb interaction. A discussion of MCT for low-density Coulomb systems is given in another publication [27].

B. Nonergodicity parameters

Some typical examples of *critical* NEPs, i.e., solutions of Eq. (11) along the phase transition line, are presented in Fig. 2. In the high-temperature limit, $f_M(q)$ becomes the Debye-Waller factor of the neutral hard-sphere system known from Ref. [2], while $f_C(q)$ approaches the corresponding Lamb-Mößbauer factor. This can be understood from the fact that $S_M(q)\to S_{PY}(q)$ and $S_C(q)\to1$ for high temperatures, where $S_{PY}(q)$ denotes the Percus-Yevick structure factor of an uncharged hard-sphere system. This static structure implies $c_C(q)\equiv0$ and $c_M(q)=2c_{PY}(q):=2[1-S_{PY}(q)^{-1}]/n$, which, inserted into Eqs. (9) and (8), leads to the high-temperature form

$$K_M^{MC}(q;t)=\frac{v_{th}^2}{2\beta^2n}\frac{1}{V}\sum_{\mathbf{k}}[k_\parallel c_{PY}(k)+p_\parallel c_{PY}(p)]^2\Phi_M(k;t)\Phi_M(p;t), \quad (33)$$

$$K_C^{\mathrm{MC}}(q;t)=\frac{v_{\mathrm{th}}^2}{\beta^2 n}\frac{1}{V}\sum_{\mathbf{k}} k_{\parallel}^2 c_{\mathrm{PY}}(k)^2\Phi_M(k;t)\Phi_C(p;t), \tag{34}$$

for the relaxation kernels. The mass-density relaxation function $\Phi_M(q;t)$ now rules the equations of motion for both charge- and mass-density relaxation. Thus, the glass transition of the liquid will be driven by the arrest of *mass*-density fluctuations only. Physically, this is due to the fact that for a large ratio of thermal to Coulomb energy, charge density becomes irrelevant for the particle dynamics and (especially at higher densities) only hard-core interactions persist. A closer look at Eqs. (33) and (34) reveals that they resemble the MCT equations of an uncharged one-component system known from Ref. [2]. Therefore, in the high-temperature limit, the relaxation function $\Phi_M(q;t)/n$ (the factor $1/n$ does not appear in the equations for the normalized functions) will approach the number-density relaxation function of a Percus-Yevick system, while $\Phi_C(q;t)/n$ becomes the corresponding incoherent relaxation function. As a consequence, $f_C(q)$ must approach the Percus-Yevick Lamb-Mößbauer factor $T^*\to\infty$.

At lower temperatures, $T^*\approx 0.01$, the charge-density NEP exhibits a peak at $q\approx q_0/2=7/(2\sigma)$, which is also visible in the Debye-Waller factor $f_{11}(q)$. It corresponds to an ordering of charges and reflects the growing influence of Coulomb interactions as temperature decreases. This peak, which was a dominant feature of Debye-Waller factors measured in the ionic glass former $2Ca(NO_3)_2 3KNO_3$ (CKN) [8], could not be reproduced by one-component models. The qualitative agreement of our SMS results with CKN scattering data suggests that the SMS is, despite its relatively simple composition, a useful model system for ionic liquids.

C. Static dielectric behavior

Via Eq. (19), the charge-density NEP $f_C(q)$ enables the calculation of the wave-number-dependent dielectric screening function $\epsilon_{\mathrm{st}}(q):=\lim_{\omega\to 0}\epsilon(q,\omega)$. In the liquid, $\epsilon_{\mathrm{st}}(q)$ is obviously completely determined by the charge-density structure factor. Idealized MCT predicts a jump of $\epsilon_{\mathrm{st}}(q)$ resulting from the discontinuity in $f_C(q)$ at the glass transition. The dielectric screening function of the glass, which is shown in Fig. 3, is therefore a nontrivial result of MCT for multicomponent liquids. The range of *negative* values of $\epsilon_{\mathrm{st}}(q)$ at intermediate q is in agreement with earlier theoretical investigations of the liquid phase of systems of charged particles [28]. A glance at the change of $\epsilon_{\mathrm{st}}(q)$ along the transition line shows that negative values appear only in an intermediate temperature and density region. According to Eq. (20), one finds $\epsilon_{\mathrm{st}}(q)<0$ if and only if $\tilde{\Omega}(q):=[\Omega_C^2(q)+K_C(q;\infty)]^{1/2}<\omega_{\mathrm{pl}}$. Thus, it is not surprising that, at very low densities, where $\Omega_C(q)$ increases monotonically with increasing q starting with ω_{pl} at zero wave number, the dielectric function takes on positive values only. The (small) positive $K_C(q;\infty)$ then guarantees a positive dielectric function. In contrast, at high densities the strong charge ordering reflected in a pronounced first peak at $q_0\approx 4.1\sigma^{-1}$ in the charge-structure factor will result in $\Omega_C^2(q)<\omega_{\mathrm{pl}}^2$ according to Eq. (6). On the other hand, at high densities the nontrivial frequency shift induced by $K_C(q;\infty)$ is large enough to compensate for the charge-ordering effect and restore $\tilde{\Omega}(q)>\omega_{\mathrm{pl}}$.

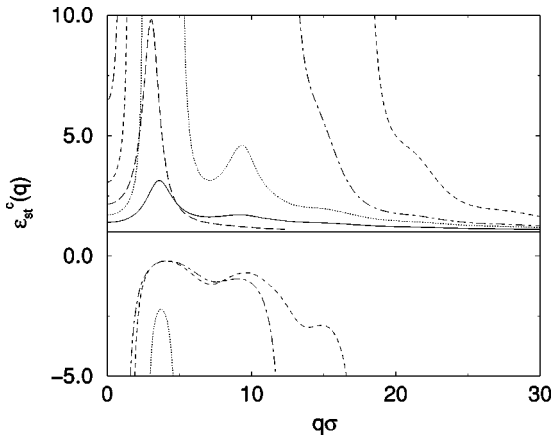

FIG. 3. Static screening function $\epsilon_{\mathrm{st}}^{\mathrm{c}}(q)$ of the RPM at melting. Curves correspond to ($\eta\approx 0.509$, $T^*\approx 0.152$) (solid line), ($\eta\approx 0.503$, $T^*\approx 0.0864$)) (dotted line), ($\eta\approx 0.477$, $T^*\approx 0.0326$)) (dashed line), ($\eta\approx 0.0743$, $T^*\approx 0.00995$) (dot-dashed line), and ($\eta\approx 0.00702$, $T^*\approx 0.0114$ (long dashed line).

The dielectric constant $\epsilon_{\mathrm{st}}(q=0)$ of the RPM was presented in an earlier publication [10]. Recently, this quantity has also been calculated in unsymmetrical systems, where, depending on the system parameters, extremely high permittivities and strong variations along the phase-transition line are predicted from MCT [29].

D. Lamb-Mößbauer factors and localization length

Our numerical results for the Lamb-Mößbauer factor $f_{\mathrm{s}}(q)$ can be approximated very well by simple Gaussians everywhere in the glass phase. Similar results have been found in previous MCT studies on other model systems [2,30].

An interesting quantity that can be calculated from the Lamb-Mößbauer factor is the localization length r_0 of a tagged particle,

$$r_0^2:=\frac{1}{3}\langle[\mathbf{r}_0^{(s)}(t=\infty)-\mathbf{r}_0^{(s)}(t=0)]^2\rangle=-\lim_{q\to 0}\frac{\partial^2 f_{\mathrm{s}}(q)}{\partial q^2}. \tag{35}$$

In the liquid, $r_0^2=\infty$ because the particle can freely move through the liquid by diffusion. The critical localization length, i.e., the value of r_0 on the glass side of the transition, is plotted in Fig. 4. This result enables a check of the empirical Lindemann criterion [31], which states that a solid should melt when the mean-square displacement of its particles exceeds 10% of the particle diameter. According to our results in Fig. 4, this statement holds for the liquid-glass transition at high and intermediate temperatures and densities, $\eta>0.1$ and $T^*>0.01$. A similar result was obtained for the neutral hard-sphere system [2] and for a Lennard-Jones liquid [32]. However, the Lindemann criterion becomes violated in the reentrant region of the phase diagram, and completely fails to predict the melting of the Wigner glass, in which the localization length can be much higher than 0.1σ [27].

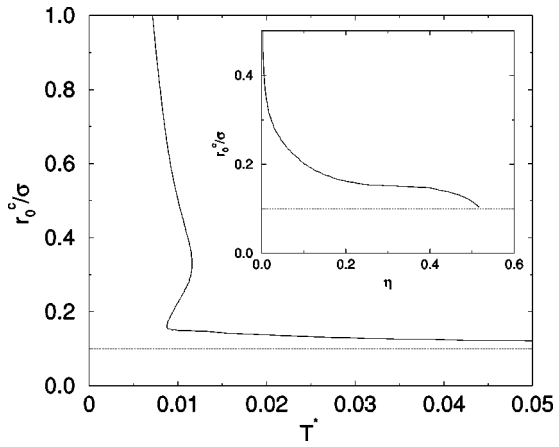

FIG. 4. Localization length r_0^c at melting as function of temperature T^* for the RPM (solid line). Dotted line: Lindemann criterion $r_0=0.1\sigma$. Inset: r_0^c as a function of η.

E. Exponent parameter

An important quantity within MCT is the Götze exponent parameter λ, which determines the exponents of the power laws appearing in the relaxation functions. For an effective one-component system like the SMS, the definition of λ found in Ref. [18] can be reinterpreted in view of the extended wave-vector indices introduced in Sec. II A by replacing each wave-number integral by a conventional wave-number integral and a sum over the mass/charge index.

Using this prescription, we have determined the exponent parameter for all transition points, and plotted the resulting function $\lambda(\eta)$ in Fig. 5. The characteristic exponents a and b, obtained from $\lambda\Gamma(1-2x)=\Gamma(1-x)^2$ with $x=a$ and $x=-b$, respectively, are also shown in the figure. The first observation is that $1/2<\lambda\leqslant 1$ for the RPM in the whole density range studied. This result supports the conjecture that the exponent parameter remains within these bounds for a large class of model systems [33]. The fact that λ does not reach unity implies that the underlying singularities are Whitney folds [33] in the whole phase diagram. At $\eta\approx 0.516$, λ approaches the limiting value $\lambda=0.735$. This value is in agreement (3% relative deviation) with the formerly found result $\lambda=0.758$ for neutral hard spheres [34].

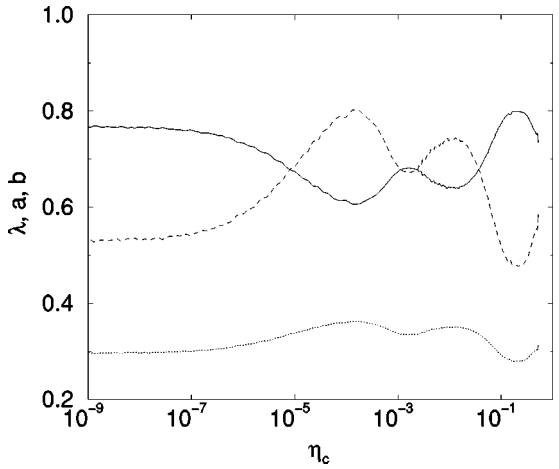

FIG. 5. Exponent parameter λ of the RPM as a function of the critical packing fraction η_c. Characteristic exponents a (dotted line) and b (dashed line).

IV. DYNAMICAL PROPERTIES

In this section we will discuss the solutions to the full time-dependent MCT equations. The partial density relaxation functions $\phi_{ss'}(q;t)$ were calculated from the specialization of Eq. (A1) to the SMS, which is equivalent to solving Eq. (2) for $\Phi_M(q;t)$ and $\Phi_C(q;t)$. In all calculations involving time-dependent quantities, 151 wave numbers and 540 time-mesh points were used.

Of special interest is, of course, the behavior of the relaxation functions as a transition point is approached from the liquid side. Since there are two thermodynamical parameters (η and T^*), each transition point (η_c, T_c^*) can be approached on various possible paths in the phase diagram. We have considered only two very simple ones: We either held $T^*=T_c^*$ fixed and varied η, or held $\eta=\eta_c$ fixed and varied T^*. It turns out that the choice of the path on which the transition is approached does not have a qualitative effect on the behavior of the relaxation functions, so that we can compare results from different transition points even if they are not approached in the same manner.

It must then be specified at which points on this path the relaxation functions are to be calculated. Since MCT predicts scaling laws $\propto|\eta-\eta_c|^x$ and $\propto|T^*-T_c^*|^x$ with different exponents x for many quantities (such as the α-relaxation time scale), it seems reasonable to choose packing fractions η_n with $|\eta_n-\eta_c|/\eta_c=a^{-n}$ for some fixed a and $n=1,2,\ldots$, if η is varied, or, correspondingly, temperatures T_n^* with $|T_n^*-T_c^*|/T_c^*=a^{-n}$ if T^* is varied. The choice $a=3$ has proven to yield an appropriate spacing between the relaxation functions if they are plotted in a common figure.

A. Coherent density relaxation

It is known that the choice of the regular parts of the relaxation kernel, $K_M^{\mathrm{reg}}(q;t)$ and $K_C^{\mathrm{reg}}(q;t)$, does not affect the long-time behavior near the glass transition, but only the damping of initial oscillations and the overall time scale of the solution [33]. Therefore, choosing a physically reasonable regular part will suffice for our purposes, keeping in mind that the short-time behavior and time scale may not be quantitatively correct. Because the regular part of the relaxation kernel does not contain mode-coupling contributions, it is assumed to decay quickly in time, $K_\mu^{\mathrm{reg}}(q;t)\approx 2\Gamma_\mu(q)\delta(t)$ for $\mu\in\{M,C\}$. Momentum conservation requires $\Gamma_M(q)\Gamma_C(q)\propto q^2$ for $q\to 0$ [20], so that one has $\Gamma_M(q)=g_{\mathrm{Br}}(q\sigma)^2$ and $\Gamma_C(q)=g_{\mathrm{Pl}}$ to lowest order in q, where realistic values for the SMS are $g_{\mathrm{Br}}\approx 0.2\omega_{\mathrm{pl}}$ and $g_{\mathrm{Pl}}\approx 0.2\omega_{\mathrm{pl}}$ [35].

In contrast to schematic models, the wave-number dependence incorporated in the present study allows new comparisons with experiments studying q-dependent quantities. The inset of Fig. 6, for example, shows the α-relaxation time of the RPM at ($\eta\approx 0.5145, T^*\approx 0.5478$) as a function of the wave number. Qualitative agreement with CKN neutron-scattering data [8] is achieved. In particular, the strong first maximum, which could not be explained using schematic models or one-component systems, is correctly reproduced

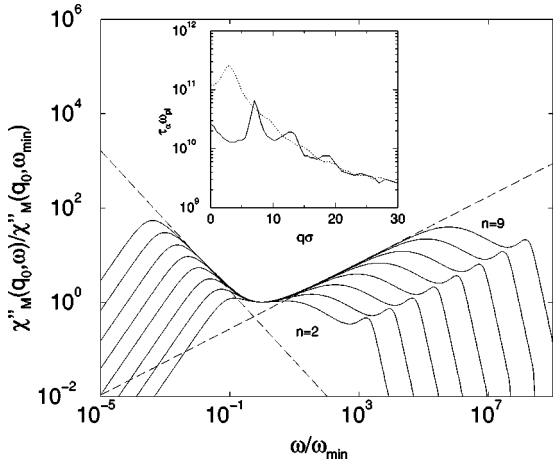

FIG. 6. Mass-density response spectrum $\chi''_M(q_0,\omega)$, $q_0 = 4\sigma^{-1}$ (solid line) as the transition at ($\eta_c \approx 0.0127$, $T_c^* \approx 0.0116$) is approached. Curves correspond to (η_c, T_n^*) with $|T_n^* - T_c^*|/T_c^* = 3^{-n}$ and $n = 2,\ldots,9$. The functions were rescaled so that the β-minima coincide. Dashed line: Power-law asymptotes $0.61\omega^a$ and $0.31\omega^{-b}$ with $a = 0.351$ and $b = 0.744$. Inset: RPM α-relaxation time τ_α as a function of the wave number at ($\eta \approx 0.5145$, $T^* \approx 0.5478$) obtained from inverse α-peak position of $\chi''_M(q,\omega)$ (solid line) and $\chi''_C(q,\omega)$ (dotted line), respectively.

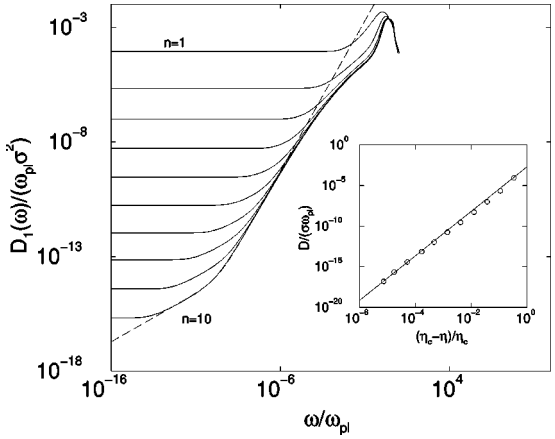

FIG. 7. Generalized diffusion coefficient $D_1(\omega)$ of the RPM as ($\eta_c \approx 0.5$, $T_c^* \approx 0.0716$) is approached. Curves correspond to (η_n, T_c^*) with $|\eta_n - \eta_c|/\eta_c = 3^{-n}$ and $n = 1,\ldots,10$. Dashed line: power law $10^{-10}\,\omega^{1-b} + 0.039\omega^{1+a}$ with $a = 0.311$ and $b = 0.580$. Inset: Diffusion coefficient $D := D_1(\omega = 0)$ (circles) together with power law $0.002[(\eta_c - \eta)/\eta_c]^\gamma$, $\gamma = 1/(2a) + 1/(2b) = 2.741$.

by the time scale obtained from the charge-density α relaxation. This result strongly supports the view that it is due to the slowing down of relaxation of *charge*-density fluctuations of the corresponding wavelength [8].

Figure 6 shows the mass-density susceptibility spectra $\chi''_M(q,\omega) := \omega \mathrm{Im}[\phi_M(q,\omega + i0)]$ at different temperatures approaching the glass transition. The individual functions were rescaled so that the minima between α and β relaxation regions fall onto one point. The plot clearly shows the asymptotic power-law solutions emerging on both sides of the minimum. The corresponding exponents a and $-b$ should, according to MCT, be independent of the wave number [18]—a prediction that was experimentally confirmed for some glass-forming substances [3], while studies on other systems revealed strong deviations [36]. However, the power laws are only *asymptotic* solutions close to the glass-transition singularity, and no statements on the range of their validity can be derived from the asymptotic formulas. We have, therefore, attempted to find this range for the SMS by putting much effort into the numerical calculations. Note, for example, that the equation of motion was solved in a time interval of 18 orders of magnitude, corresponding to relaxation times ranging from picoseconds to over ten years.

The present study yields three major results concerning the validity of the asymptotic solutions. First, the range of validity strongly depends on the observed function. While, for example, the shear viscosity in Fig. 8 clearly shows both power laws, the dynamical conductivity, Fig. 10, exhibits hardly any α-relaxation power law. Moreover, the power law that appears already very far away from the transition is the power-law divergence of the α-relaxation time scale $\tau_\alpha \propto (T^* - T_c^*)^{-\gamma}$, for example, in Fig. 8. This theoretical result complies well with the fact that the power-law behavior is indeed observed experimentally in a range of temperatures starting rather far from the actual transition. Upon further cooling, other processes not included in the present theory (e.g., hopping diffusion) mask this power law and lead to a different temperature dependence, such as a Vogel-Fulcher law.

Finally, Fig. 6 shows that the exponents of the power laws right and left of the β minimum become clearly visible only very close to the transition. The attempt to determine a and b from spectra too far away from the transition, e.g., for $n = 2$ or 3, would obviously lead to a considerable error. This result casts doubt on whether the β-minimum rescaling is suitable for a precise determination of the exponent parameter from experimental data.

B. Tagged particle relaxation

In the calculation of the tagged particle density relaxation functions from Eqs. (14) and (15), the regular memory kernel was assumed to be of the form $K_s^{reg}(q;t) = 2\Gamma_s(q)\delta(t)$. The magnitude of $\Gamma_s(q)$ was found to affect the short-time behavior of the tagged particle relaxation functions, and—in contrast to the coherent $K^{reg}(q;t)$—not their overall time scale. $\Gamma_s(q) = 10\omega_{pl}$ was chosen for the calculations, where the nonvanishing value at $q = 0$ reflects that the tagged particle momentum is not conserved.

Qualitatively, $\phi_s(q;t) := \Phi_s(q;t)/\Phi_s(q;t=0)$ exhibits the same behavior as its coherent counterparts. A more interesting quantity is the frequency-dependent diffusion coefficient, which can be obtained from the tagged particle relaxation kernel by

$$D_s(\omega) = \mathrm{Im}\left\{ \frac{-v_{th}^2}{\omega + K_s(q=0,\omega+i0)} \right\}. \tag{36}$$

This function has been plotted in Fig. 7. The high-frequency behavior is dominated by a peak at microscopic frequencies, which is due to microscopic oscillations in short-lived cages formed by next neighbors. In the frequency ranges of β and α relaxation, the diffusion constant exhibits power laws with exponents $1-b$ and $1+a$, respectively. Their appearance can be explained by the small-frequency behavior of $\phi_s(q,z)$

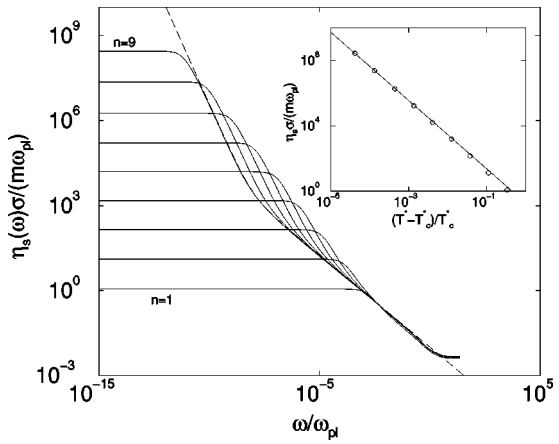

FIG. 8. Generalized shear viscosity $\eta_s(\omega)$ (solid line) as ($\eta_c \approx 0.0127$, $T_c^* \approx 0.0116$) is approached. Curves correspond to (η_c, T_n^*) with $|T_n^* - T_c^*|/T_c^* = 3^{-n}$ and $n = 1, \ldots, 9$. Dashed line, power-law function $0.01\omega^{a-1} + 1.4\times 10^{-11}\omega^{-b-1}$ with $a = 0.351$, $b = 0.744$. Inset: Shear viscosity η_s (circles) together with power law $0.18[(T^* - T_c^*)/T_c^*]^{-\gamma}$, $\gamma = 1/(2a) + 1/(2b) = 2.097$.

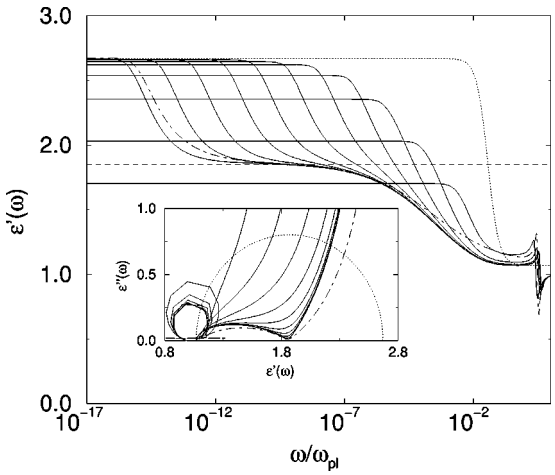

FIG. 9. Real part of dielectric function $\epsilon(\omega)$ of RPM as ($\eta_c \approx 0.5$, $T_c^* \approx 0.0716$) is approached. Curves correspond to (η_n, T_c^*) with $|\eta_n - \eta_c|/\eta_c = 3^{-n}$ and $n = 1, \ldots, 11$. Dashed horizontal line, expected critical dielectric constant $\epsilon_{st}^c = 1/f_C(q=0)$; dotted line, Debye model Eq. (23); dot-dashed line, extended model Eq. (28); inset: same data in as Cole-Cole plot.

[18]. The inset of Fig. 7 shows the ($\omega = 0$)-diffusion constant D as the glass transition is approached. It obviously decreases towards zero exhibiting the predicted power-law behavior with exponent γ, i.e., $D \propto (\eta_c - \eta)^\gamma$ [18].

C. Shear viscosity

The generalized shear viscosity $\eta_s(\omega)$ can be related to the transversal current relaxation kernel by

$$\eta_s(\omega) = mn \lim_{q\to 0} \frac{\mathrm{Im}[K_\perp(q, \omega + \mathrm{i}0)]}{q^2}. \tag{37}$$

$K_\perp(q, \omega + \mathrm{i}0)$ has been calculated from Eq. (16) with $K_\perp^{\mathrm{reg}}(q;t) = 2\Gamma_\perp(q)\,\delta(t)$. Similarly to the incoherent regular relaxation kernel, $\Gamma_\perp(q)$ is found to affect the high-frequency part of η_s only; $\Gamma_\perp(q) = \omega_{pl}$ was chosen. A set of generalized viscosities is plotted in Fig. 8. Clearly, the shear viscosity $\eta_s := \eta_s(\omega = 0)$ increases dramatically close to the transition point, signaling the divergence of the viscosity at a critical temperature T_c^* predicted by idealized MCT. $\eta_s(\omega) \propto \mathrm{Im}[K_M^T(q, \omega)]$ is expected to show power-law behavior in the α- and β-relaxation regimes with the exponents $a - 1$ and $-b - 1$ [18], respectively, which is reproduced by the numerical solution shown in Fig. 8.

D. Dynamical dielectric properties

Having characterized the system's response to static electric fields in Sec. III C, knowledge of the time-dependent relaxation functions enables the calculation of the *frequency-dependent* dielectric function of the supercooled liquid at $q = 0$, $\epsilon(\omega)$, via Eq. (17).

The real part of $\epsilon(\omega)$, which is plotted in Fig. 9, shows a rather complex frequency dependence near the glass transition. The resonance near ω_{pl} can be attributed to plasma oscillations. Following at lower frequencies, there appears a range of about two decades with very little variation of $\epsilon(\omega)$. This is the high-frequency dielectric constant ϵ_∞ introduced in Sec. II B. It is followed by two steps, corresponding to the β- and α-relaxation processes. This qualitative behavior at low frequencies is in agreement with experiments, e.g., on the glass former phenyl salicylate (salol) [37].

On the other hand, the imaginary part $\epsilon''(\omega)$ diverges for $\omega \to 0$ in the SMS, while it approaches zero in the salol experiment. This discrepancy must be attributed to the fact that salol is a liquid of *neutral*, *dipolar* molecules with a vanishing (or extremely small) dc-conductivity, while the SMS consisting of mobile charged particles still has an appreciable dc conductivity in the supercooled phase. The only dielectric response that a liquid of neutral molecules can perform is the reorientation of the molecular dipole moments, which, at very low external field frequencies, happens without a phase shift relative to the external field: $\epsilon''(\omega) = 0$ for $\omega \to 0$. In the SMS, there are no permanent dipole moments, and thus the response to static fields will be a separation of charges. The SMS liquid can, therefore, completely screen off any external field, which implies an infinite ($\omega = 0$) value of the dielectric function.

The plot also allows a comparison of the models of dielectric behavior discussed in Sec. II B. Obviously, the simple Ansatz Eq. (23) is only a very crude approximation of the dielectric function not capable of describing the two-step relaxation behavior as it corresponds to the special case $\beta_1 = 1$ of the more general model Eq. (28).

To match the more elaborate empirical formula Eq. (28) (which was recently successfully used to fit experimental data [22]) to our MCT calculation, we now determine the parameters of this ansatz for the $n = 11$ MCT solution. The plateau values $\epsilon_\infty \approx 1.07$, $\epsilon_{st}^c \approx 1.85$, and $\epsilon \approx 2.67$, are taken from Fig. 9 and the dc conductivity $\sigma_0/(\epsilon_0\omega_{pl}) = 1.9 \times 10^{-15}$ from Fig. 10. These values then fix the parameters τ_1, β_1, and $\tilde{f}$ of the model Eq. (28) via Eqs. (30) and (32) yielding $\tau_1 = 1.31 \times 10^{15}/\omega_{pl}$, $\beta_1 = 0.342$, and $\tilde{f} = 0.082$. For the shorter relaxation time we estimate $\tau_2 \approx 1.2/\omega_{pl}$ from Fig. 9 (or from a plot of $\mathrm{Im}[\epsilon(\omega)]$), and finally, for the Cole-Cole exponent we choose $\beta_2 = a = 0.311$, because it is

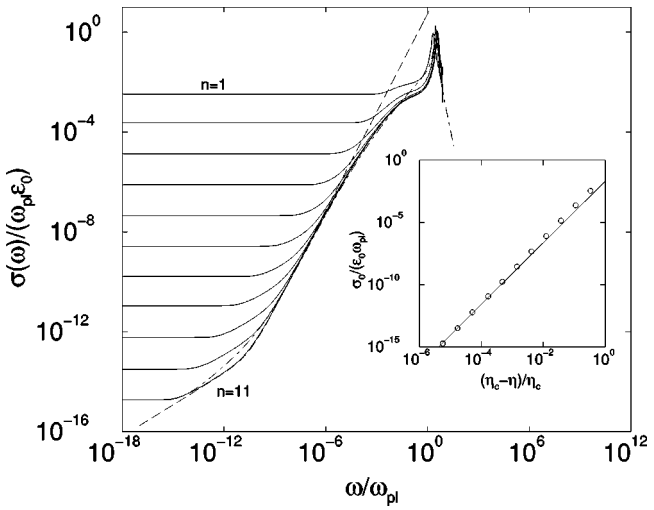

FIG. 10. Real part of dynamical conductivity $\sigma(\omega)$ of RPM as transition point ($\eta_c \approx 0.5$, $T_c^* \approx 0.0716$) is approached. Curves correspond to (η_n, T_c^*) with $|\eta_n - \eta_c|/\eta_c = 3^{-n}$ and $n = 1, \ldots, 11$. Dashed line, Power law $5.1\omega^{a+1} + 2.5\times 10^{-9}\omega^{1-b}$ with $a = 0.311$ and $b = 0.580$. Dot-dashed line, Conductivity obtained from extended model Eq. (28). Inset: dc conductivity σ_0 (circles) as a function of distance from the transition. Solid line, Power law $0.02[(\eta_c - \eta)/\eta_c]^\gamma$, $\gamma = 1/(2a) + 1/(2b) = 2.741$.

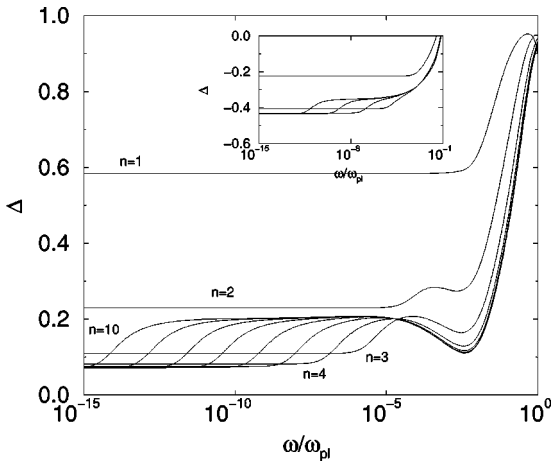

FIG. 11. Deviation parameter Δ of the RPM as a function of frequency ω as ($\eta_c \approx 0.5$, $T_c^* \approx 0.0716$) is approached. Curves correspond to (η_n, T_c^*) with $|\eta_n - \eta_c|/\eta_c = 3^{-n}$ and $n = 1, \ldots, 10$. Inset: Δ as ($\eta_c \approx 0.0127$, $T_c^* \approx 0.0116$) is approached. Curves correspond to (η_c, T_n^*) with $|T_n^* - T_c^*|/T_c^* = 3^{-n}$ and $n = 1, \ldots, 9$.

known that in the β-relaxation region the MCT solution for the charge-density response takes on the Cole-Cole form [7]. The resulting curve presents a very reasonable fit to the MCT solution. This is not only true for $\epsilon'(\omega)$ but—with the same set of parameter values—it is also true for $\epsilon''(\omega)$ as well as for $\sigma(\omega)$. Especially in the β region $10^{-3} > \omega/\omega_{pl} > 10^{-9}$, the model gives a perfect description of the MCT results. We note, however, that the exponent β_1, which is determined by the two plateau values ϵ^{II} and ϵ^{III}, does not come out to be equal to the MCT exponent b. This demonstrates that in the α-relaxation region the MCT solution does not take on the Cole-Davidson form exactly (in contrast to the Cole-Cole form of the β-relaxation region).

The inset of Fig. 9 shows the dielectric function in a Cole-Cole diagram, where the complex $\epsilon(\omega) = \epsilon'(\omega) + i\epsilon''(\omega)$ is plotted as a path in the (ϵ', ϵ'') plane by varying the frequency ω. At intermediate frequencies, the Cole-Cole plot exhibits a ''squeezed'' half circle typical for the stretched relaxation of glass-forming liquids. The simple exponential (Debye) relaxation of charge-density fluctuations corresponds to the circle included in the figure. The stretched β relaxation leads to a much flatter Cole-Cole plot than predicted by a Debye model. Note that the right wing of the Cole-Cole plot may be extrapolated onto the abscissa to obtain the critical dielectric constant $\epsilon_{st}^c \approx 1.85$. On the left side of the Cole-Cole plot, the curve approaches the high-frequency dielectric constant ϵ_∞ before it exhibits an additional circle corresponding to the plasma resonance. Most experiments measure the dielectric function at frequencies below this resonance only.

E. Dynamical conductivity

Figure 10 shows the real part of the dynamical conductivity obtained from the dielectric constant via Eq. (22). The dc conductivity $\sigma_0 := \sigma(\omega = 0)$ vanishes as the glass transition is approached. Its behavior close to the transition is again given by a power law with exponent γ, which is shown in the inset of Fig. 10. The plot shows that various power laws dominate the frequency dependence of $\sigma(\omega)$. They can be understood analogously to the power laws in the diffusion coefficient [18]. One finds the exponents $1 + a$ and $1 - b$, which are clearly reproduced by our numerical result. Although the RPM is the simplest possible two-component model for an ionic liquid, qualitative agreement is achieved with measurements on real ionic glass formers (e.g., [38,39]). It is obvious that the frequency dependence of the conductivity is very similar to that of the diffusion coefficient in Fig. 7. This point will be discussed in the next section.

F. Nernst-Einstein relation

The Nernst-Einstein relation is based on the assumption that cross correlations of the velocities of different particles can be neglected [40]. This results in a relation between conductivity and diffusion coefficient,

$$\sigma(\omega) = \frac{n(Ze)^2}{k_B T} D(\omega)(1 - \Delta). \tag{38}$$

The quantity Δ is a (possibly frequency-dependent) deviation parameter, which has been determined experimentally for several molten salts. For $\omega = 0$, it was found to take on mostly positive values, for example, 0.08 for NaI or 0.43 for $LiNO_3$ [41,40].

Since MCT yields that D and σ_0 both vanish as $(T^* - T_c^*)^\gamma$ near the transition temperature T_c^*, it is clear that idealized MCT predicts $D \propto \sigma_0$. Next to this result, there are two interesting questions that may be answered by our calculation. The first is in how far the frequency dependence of $D(\omega)$ will be the same as that of $\sigma(\omega)$, and the other is whether MCT is able to predict reasonable values for the deviation parameter Δ in the RPM.

Figure 11 shows the deviation parameter Δ as a function of frequency. A first observation is that—except at micro-

scopic frequencies—it is only very weakly frequency dependent. This corresponds to the statement that MCT predicts a rather general validity of Eq. (38) for a large range of frequencies even close to the glass transition. The weak frequency dependence may be understood analytically by considering that MCT predicts the same power-law exponents for $D(\omega)$ and $\sigma(\omega)$ in the α- and β-relaxation regime. The deviation parameter takes on values of about $0.07,\ldots,0.5$ depending on the separation from the glass transition, which is in agreement with the experimental values mentioned above.

Deeper in the liquid ($n=1$), the deviation parameter is rather large, $\Delta\approx 0.6$, and it clearly decreases as the transition is approached. This result may be interpreted in terms of the formation of short-lived ionic complexes, which contribute only to the diffusive flux but not to the electric current [40]. The probability for a particle to be dragged along by another one of opposite charge is obviously higher in the ''normal'' liquid than in the highly viscous supercooled state. Thus, the conductivity should be comparably smaller far away from the transition, resulting in a rather large deviation parameter Δ.

The above results for Δ are confirmed in another calculation at a lower density shown in the inset of Fig. 11. The only difference is that Δ is generally shifted towards smaller values. In particular, Δ is negative near this transition point.

G. Stokes-Einstein relation

The Stokes-Einstein relation establishes a connection between diffusion coefficient and shear viscosity. It reads

$$D=\frac{k_{\mathrm{B}}T}{\eta_{\mathrm{s}}BR}, \tag{39}$$

where the quantity B is a numerical constant ($B=4\pi$ for ''slip'' and $B=6\pi$ for ''stick'' boundary conditions at the surface of the diffusing particle) and R is the Stokes-Einstein radius of the particles. Equation (39) was originally derived for the diffusion of a large Brownian particle [42], but turned out to be a good approximation even for self-diffusion in viscous liquids, i.e., when R is the particle or molecule radius.

Near the glass transition, however, the Stokes-Einstein relation tends to underestimate the diffusion constant for some glass formers. These deviations from Eq. (39) may be interpreted as deviations of an effective (Stokes-Einstein) radius R from the particle radius $\sigma/2$. While a molecular-dynamics study of a supercooled binary soft-sphere system showed $R\approx\sigma/2$ until the hopping diffusion regime was reached [14], other investigations (cited e.g., in Ref. [13]) reported systematic deviations of the Stokes radius from the particle radius. An *ad-hoc* modification suggested to remedy this failure leads to the fractional Stokes-Einstein relation $D\propto(T/\eta)^{\xi}$ with $0<\xi\leqslant 1$ [43].

Within the framework of MCT, D and η_{s} are calculated separately along different lines. It is, therefore, predestined for giving nontrivial results on the Stokes-Einstein radius R near the glass transition. The MCT power-law exponents governing the behavior of D and $1/\eta_{\mathrm{s}}$ close to the transition [18] guarantee that our results on R will converge towards a constant as a glass-transition point is approached (i.e., $\xi=1$). We argue that hopping diffusion, which is neglected in the idealized MCT used here, may cause deviations (such as exponents $\xi<1$) from this behavior close to the transition in real systems.

We have calculated the MCT estimate of the Stokes-Einstein radius at the high- and intermediate-density glass transition of the SMS. While its value at the high-density transition $\eta\approx 0.5$ is approximately equal to the hard-core radius ($R\approx 1.46\sigma/2$ for $B=6\pi$), there are strong deviations at the lower-density transition near $\eta\approx 0.01$, where $R\approx 58.1\sigma/2$. Extremely large Stokes radii have recently also been found in a MCT study of a one-component charged hard-sphere system with neutralizing background [27] and appear to be a typical feature of low-density Coulomb systems. The effective ''inflation'' of the charged particles can be interpreted as a result of the long-ranged Coulomb forces dominating the interaction at low densities. Our results suggest that, at lower temperature and density, diffusion and shear viscosity of supercooled Coulomb liquids will exhibit properties similar to those of nonsupercooled liquids with much larger particles.

V. CONCLUSION

In this paper we have discussed the glass transition of the RPM, a symmetrical binary mixture of charged hard spheres, using MCT. The full wave-number-dependent MCT equations for a SMS were shown to be formally equivalent to those of MCT for a *one-component* liquid. The numerical solutions obtained in our calculations could, therefore, be checked using the predictions derived from one-component MCT. A number of interesting results were obtained for the RPM glass transition.

(a) The RPM glass transition at high densities is predicted to occur at a localization length of about 10% of the particle diameter, confirming Lindemann criterion for melting.

(b) The exponent parameter λ, which could be determined only at single transition points in MCT studies so far, was calculated along the whole phase transition line. It is found to vary continuously between 0.8 and 0.6.

(c) The double-peak structure of the Debye-Waller factor and of the primary relaxation time of the ionic glass former CKN were qualitatively reproduced by the RPM calculations.

(d) The Nernst-Einstein relation (and its frequency-dependent generalization) are predicted to be fulfilled for the RPM near the glass transition.

(e) The MCT results at high densities show good agreement with the Stokes-Einstein relation. At lower densities, MCT predicts a Stokes radius that exceeds the hard-core radius by a factor of about 50. Similar results have been obtained in a recent study on a hard-sphere jellium fluid [27], which indicates that they are related to the long-ranged Coulomb interaction. We argue that these qualitative results are relevant despite the use of *idealized* MCT in our study, since they remain valid in the nonasymptotic region further away from the transition, which idealized MCT is widely accepted to describe accurately.

This paper has given a detailed account of the MCT results for the glass transition of the SMS. However, it is still

only a starting point for the investigation of more general supercooled ionic mixtures. Much work remains to be done in this field analytically as well as numerically, but we believe that the study of these systems will be rewarding in two ways: On the one hand, it is hoped to lead to progress in the physically and technologically interesting field of ionic liquids and glasses. On the other hand, the application of established theories for simple liquids (such as MCT) to ionic multicomponent systems provides a means of testing, and possibly improving, the theoretical basis of our understanding of the glass transition.

ACKNOWLEDGMENT

This work was supported by the Deutsche Forschungsgemeinschaft (SFB 337).

APPENDIX A: "SHORTCUT" DERIVATION OF MODE-COUPLING APPROXIMATION

This section contains an oversimplified derivation of the MCA for multicomponent liquids. A much more elaborate approach, which, however, yields the same result, can be found in Refs. [44,7].

We will formulate the derivation for a classical S-component liquid, which we assume to be homogeneous and isotropic. Its particles (of species s and s') interact via a rotationally invariant, additive pair potential $v_{ss'}(r)$. We will use the partial number densities $N^{(s)}(\mathbf{q}) := \sum_{j=1}^{N_s} \exp[-i\mathbf{q}\cdot\mathbf{r}_j^{(s)}]/\sqrt{N_s}$ as the basic variable set. Via the Mori-Zwanzig projector-operator formalism [16,17], a formally exact generalized-oscillator equation of motion for the matrix of relaxation functions $\Phi_{ss'}(q,z)$ (see Sec. II A for a definition) is derived,

$$\Phi(q,z) = -\left[z + \frac{-1}{z + K(q,z)} \Omega^2(q) \right]^{-1} \Phi(q;t=0), \tag{A1}$$

with the frequency matrix $\Omega^2_{ss'}(q) := q^2/\beta m_s [S(q)]^{-1}_{ss'}$ and the relaxation kernel matrix

$$K_{ss'}(q,z) := \sum_{\sigma=1}^{S} \left[N^{(s)}(\mathbf{q}) \middle| \mathcal{L}^2 \frac{\mathcal{Q}}{\mathcal{Q}L\mathcal{Q} - z} \mathcal{L}^2 \middle| N^{(\sigma)}(\mathbf{q}) \right] \times [\Omega^2(q)^{-1}]_{\sigma s'} \tag{A2}$$

$$= m_s (J_\parallel^{(s)}(\mathbf{q}) | \mathcal{L}\mathcal{Q} e^{-i t \mathcal{L}\mathcal{Q}} \mathcal{L} | J_\parallel^{(s')}(\mathbf{q})), \tag{A3}$$

where $\mathcal{L}$ denotes the Liouvillian, $J^{(s)}(\mathbf{q}) := \sum_{j=1}^{N_s} \mathbf{q}\cdot\mathbf{p}_j^{(s)} \exp[-i\mathbf{q}\cdot\mathbf{r}_j^{(s)}]/(q\sqrt{m_s N_s})$ is the longitudinal current density, and m_s is the mass of a particle of species s. The operator $\mathcal{Q}$ introduced in Eq. (A2) is a projector onto the subspace orthogonal to that spanned by all $N^{(s)}(\mathbf{q})$ and $\mathcal{L}N^{(s)}(\mathbf{q})$ in the space of dynamical variables. Equation (A3) was obtained by employing the continuity equation and the f-sum rule. The $(t=0)$ value of the relaxation functions can be expressed in terms of the partial density static structure factors, $\Phi(q;t=0) = \beta S(q)$.

The next step is to replace the two outer Liouville operators in Eq. (A3) by their potential part $\mathcal{L}_{\rm pot} := i\{H_{\rm pot}, \cdot\}$, where $H_{\rm pot} := \sum_{s,s'=1}^{S} \sum_{i=1}^{N_s} \sum_{j=1}^{N_{s'}} v_{ss'}(|\mathbf{r}_i^{(s)} - \mathbf{r}_j^{(s')}|)/2$ is solely due to interaction effects. At times exceeding the microscopic time scale, $\mathcal{L}_{\rm pot}$ is expected to play the dominant role, while the effect of the remaining free-particle Liouvillian $\mathcal{L} - \mathcal{L}_{\rm pot}$ may be neglected. The variable $\mathcal{L}_{\rm pot} J_\parallel^{(s)}(\mathbf{q})$ can be evaluated explicitly to yield $-\sum_{\mathbf{k}} \sum_{\sigma=1}^{S} \sqrt{N_\sigma} k_\parallel v_{s\sigma}(k) N^{(s)}(\mathbf{q}-\mathbf{k}) N^{(\sigma)}(\mathbf{k})/(V m_s)$, where the symmetry of the interaction potential, $-v_{\mu\sigma}(k) = v_{\mu\sigma}(-k) = v_{\sigma\mu}(-k)$, has been used. The bare interaction potential is then screened by $v_{ss'}(q) \approx -k_B T c_{ss'}(q)$. The last step is to eliminate the two-mode variables that originate from $\mathcal{L}_{\rm pot} J_\parallel^{(s)}(\mathbf{q})$. Since we will be interested in the long-time behavior of relaxation functions and friction kernels, a factorization of the two-mode correlations appearing in the relaxation kernel,

$$\begin{aligned} &\beta [N^{(s)}(\mathbf{q}-\mathbf{k}) N^{(\sigma)}(\mathbf{k}) | \mathcal{Q} e^{-i t \mathcal{Q}L\mathcal{Q}} | N^{(s')}(\mathbf{q}-\mathbf{p}) N^{(\sigma')}(\mathbf{p})] \\ &\quad \approx \Phi_{ss'}(|\mathbf{q}-\mathbf{k}|;t) \Phi_{\sigma\sigma'}(k;t) \delta_{\mathbf{p},\mathbf{k}} \\ &\qquad + \Phi_{s\sigma'}(|\mathbf{q}-\mathbf{k}|;t) \Phi_{\sigma s'}(k;t) \delta_{\mathbf{p},\mathbf{q}-\mathbf{k}} \end{aligned} \tag{A4}$$

seems appropriate. Note that the effect of $\mathcal{Q}$ was restricted to the projection onto the subspace of two-mode variables. The result is a relaxation kernel of the form

$$\begin{aligned} K^{\rm MC}_{ss'}(q;t) \approx \frac{1}{\beta^3 m_s} \frac{1}{V} \sum_{\mathbf{k}} \sum_{\sigma,\sigma'=1}^{S} &[k_\parallel^2 \sqrt{n_\sigma} c_{s\sigma}(k) \\ &\times \sqrt{n_{\sigma'}} c_{s'\sigma'}(k) \Phi_{ss'}(|\mathbf{q}-\mathbf{k}|;t) \Phi_{\sigma\sigma'}(k;t) \\ &+ k_\parallel (q - k_\parallel) \sqrt{n_{\sigma'}} c_{s'\sigma'} \\ &\times (|\mathbf{q}-\mathbf{k}|) \sqrt{n_\sigma} c_{s\sigma}(k) \Phi_{s\sigma'}(|\mathbf{q}-\mathbf{k}|;t) \\ &\times \Phi_{\sigma s'}(k;t)]. \end{aligned} \tag{A5}$$

This relaxation kernel contains mode-coupling contributions only. All other influences are summarized in a regular part $K^{\rm reg}(q;t)$,

$$K(q;t) = K^{\rm reg}(q;t) + K^{\rm MC}(q;t), \tag{A6}$$

which is assumed to decay very quickly in time. Equation (A5) is equivalent to the matrix Eq. (31) of Ref. [20].

A simplified version of the MCA for the tagged particle and for the transversal current relaxation kernels can be found in complete analogy to the derivation presented above.

APPENDIX B: TRANSFORMATION OF BASIS VARIABLES

In this appendix we collect the formulas for the transformation of MCT equations from partial number densities to another set of basis variables.

Instead of the variables $N^{(s)}(\mathbf{q})$, a set $A^{(s)}(\mathbf{q}) := \sum_{s'} N^{(s')}(\mathbf{q}) [T^\dagger(q)]_{s's}$ of linear combinations of the partial densities will now be considered. The transformation matrix $T(q)$ is required to be nonsingular. Then, the corresponding matrix of relaxation functions $\check{\Phi}_{ss'}(q;t) := \Phi_{A^{(s)}(\mathbf{q}) A^{(s')}(\mathbf{q})}(t)$ is given by

$$\check{\Phi}(q;t)=T(q)\Phi(q;t)T^{\dagger}(q). \tag{B1}$$

The equation of motion for the matrix $\check{\Phi}(q,z)$ will have the same form as Eq. (A1),

$$\check{\Phi}(q,z)=-\left[z+\frac{-1}{z+\check{K}(q,z)}\check{\Omega}^2(q)\right]^{-1}\check{\Phi}(q;t=0), \tag{B2}$$

only with transformed frequency matrix and memory kernel,

$$\check{\Omega}^2(q)=T(q)\Omega^2(q)T(q)^{-1}, \tag{B3}$$

$$\check{K}(q,z)=T(q)K(q,z)T(q)^{-1}. \tag{B4}$$

Note that, since $T(q)$ is nonsingular, the projection operator $\mathcal{Q}$ in Eq. (A2) does not depend on the specific linear combination $A^{(s)}$ of the partial densities. Consequently, the reduced evolution operator $\mathcal{Q}e^{-it\mathcal{L}Q}$ is also independent of the choice of the linear combination. Therefore, merely the relaxation functions appearing in Eq. (A5) have to be transformed according to Eq. (B1) to obtain a new MCA relaxation kernel in terms of the transformed relaxation functions.

APPENDIX C: STATIC STRUCTURE OF THE RPM

In this appendix we include the RPM static structure factors within the MSA [24] for reference. For the SMS, the implicit equation to be solved for the MSA static structure of general charged two-component systems is trivial, so that the SMS structure factors can be given in explicit form. The charge-structure factor depends on η/T^* only. Abbreviating $\hat{q}:=q\sigma$ (where σ is the hard-sphere diameter), $x:=96\eta/T^*$, and $w:=\sqrt{1+\sqrt{x}}-1$, one finds

$$S_C(\hat{q})=\frac{\hat{q}^4/2}{2\hat{q}^4-4w^2-4w^3+x+2w^3\hat{q}\sin(\hat{q})+(4w^2+4w^3-x+2\hat{q}^2w^2)\cos(\hat{q})} \tag{C1}$$

$$=\frac{\hat{q}^2}{x}\left[1+\frac{\hat{q}^2}{12x}(x-48+20w^2+4w^3)+O(\hat{q}^4)\right]. \tag{C2}$$

The mass structure factor is temperature-independent:

$$S_M(\hat{q})=[\hat{q}^6(\eta-1)^4]\{\hat{q}^6(\eta-1)^4+72\eta^2[\hat{q}^2(2+\eta)^2+4(1+2\eta)^2]-12\eta\cos(\hat{q})[24\eta(1+2\eta)^2-6\hat{q}^2\eta(7\eta^2+4\eta-2)$$
$$+\hat{q}^4(\eta-1)^2(\eta+2)]+24\eta\hat{q}\sin(\hat{q})[\hat{q}^2(\eta-1)(5\eta^2+5\eta-1)-12\eta(1+2\eta)^2]\}^{-1} \tag{C3}$$

$$=\frac{(\eta-1)^4}{(1+2\eta)^2}+\frac{\eta(\eta-1)^4(4\eta^2-11\eta+16)}{20(1+2\eta)^4}\hat{q}^2+\mathcal{O}(\hat{q}^4). \tag{C4}$$

[1] E. Leutheusser, Phys. Rev. A **29**, 2765 (1984).
[2] U. Bengtzelius, W. Götze, and A. Sjölander, J. Phys. C **17**, 5915 (1984).
[3] H.Z. Cummins, G. Li, Y.H. Hwang, G.Q. Shen, W.M. Du, J. Hernandez, and N.J. Tao, Z. Phys. B **103**, 501 (1997).
[4] J. Bosse and U. Krieger J. Phys. C , **19**, L609 (1986).
[5] U. Krieger and J. Bosse, *Proceedings of the NATO Advanced Study Institute on Amorphous and Liquid Materials, Passo del Mendola, Italy, 1985*, Vol. 118 of *NATO Advanced Study Institute, Series E*, edited by E. Lüsher, C. Fritsch, and G. Jacucci (Martinus Nijhoff, Boston, MA, 1987).
[6] U. Krieger and J. Bosse, Phys. Rev. Lett. **59**, 1601 (1987).
[7] J. Bosse and M. Henel. Ber. Bunsenges. Phys. Chem. **95**, 1007 (1991).
[8] F. Mezei, W. Knaak, and B. Farago, Phys. Scr. **T19**, 363 (1987).
[9] W. Götze and R. Haussmann, Z. Phys. B **72**, 403 (1988).
[10] J. Bosse and S.D. Wilke. Phys. Rev. Lett. **80**, 1260 (1998).
[11] D. Bonn, H. Tanaka, G. Wegdam, H. Kellay, and J. Meunier Europhys. Lett. **45**, 52 (1999).
[12] H. Thomas, G.E. Morfill, V. Demmel, J. Goree, B. Feuerbacher, and D. Möhlmann, Phys. Rev. Lett. **73**, 652 (1994).
[13] J.A. Hodgdon and F.H. Stillinger, Phys. Rev. E **48**, 207 (1993).
[14] J.L. Barrat, R.N. Roux, and J.-P. Hansen, Chem. Phys. **49**, 197 (1990).
[15] C.T. Moynihan, N. Balitactac, L. Boone, and T.A. Litovitz, J. Chem. Phys. **55**, 3013 (1971).
[16] H. Mori. Prog. Theor. Phys. **33**, 399 (1965); **34**, 399 (1965).
[17] R. Zwanzig, in *Lectures in Theoretical Physics*, edited by W. Brittin and L. Dunham (Wiley-Interscience, New York, 1961) Vol. 3.
[18] W. Götze, Z. Phys. B **60**, 195 (1985).
[19] J. Bosse and J.S. Thakur, Phys. Rev. Lett. **59**, 998 (1987).
[20] J. Bosse, Z. Phys. B **103**, 357 (1997).
[21] P. C. Martin, in *Problème à N Corps*, edited by C. de Witt and R. Balian, Gordon and Breach, New York, 1968), p. 37.
[22] M. Soltwisch, G. Ruocco, B. Balschun, J. Bosse, V. Mazzacurati, and D. Quitmann, Phys. Rev. E **57**, 720 (1998).
[23] W. Götze and L. Sjögren, J. Phys. C **21**, 3407 (1988).
[24] E. Waisman and J.L. Lebowitz, J. Chem. Phys. **56**, 3093 (1972).

[25] S.K. Lai, W.J. Ma, W.van Megen, and I.K. Snook, Phys. Rev. E **56**, 766 (1997).
[26] S. Khan, T.L. Morton, and D. Ronis, Phys. Rev. A **35**, 4295 (1987).
[27] S.D. Wilke and J. Bosse, Phys. Rev. E **59**, 1968 (1999).
[28] A. Chandra and B. Bagchi, J. Chem. Phys. **91**, 3057 (1989).
[29] H. C. Chen, S. D. Wilke, and J. Bosse, Phys. Rev. B (to be published).
[30] U. Bengtzelius, Phys. Rev. A **34**, 5059 (1986).
[31] F.A. Lindemann, Phys. Z. **11**, 609 (1910).
[32] U. Bengtzelius, Phys. Rev. A **33**, 3433 (1986).
[33] W. Götze, in *Liquids, Freezing, and the Glass Transition*, edited by D. Levesque, J. P. Hansen, and J. Zinn-Justin, (North-Holland, Amsterdam, 1991), Vol I, p. 289.
[34] J.L. Barrat, W. Götze, and A. Latz, J. Phys.: Condens. Matter **1**, 7163 (1989).
[35] J. Bosse and T. Munakata Phys. Rev. A **25**, 2763 (1982).
[36] A. Hofmann, F. Kremer, and E.W. Fischer, Physica A **201**, 106 (1993).
[37] P.K. Dixon, L. Wu, S.R. Nagel, B.D. Williams, and J.P. Carini, Phys. Rev. Lett. **65**, 1108 (1990).
[38] R. Bose, R. Weiler, and B. Macedo, Phys. Chem. Glasses **11** (1970).
[39] K. Funke, J. Hermeling, and J. Kümpers, Z. Naturforsch., A: Phys. Sci. **43**, 1094 (1988).
[40] J.-P. Hansen and I.R. McDonald, Phys. Rev. A **11**, 2111 (1975).
[41] N. H. March and M. P. Tosi, *Coulomb Liquids*, (Academic Press, London, 1984).
[42] A. Einstein, Ann. Phys. (Leipzig) **17**, 549 (1905).
[43] A. Voronel, E. Veliyulin, V.Sh. Machavariani, A. Kisliuk, and D. Quitmann, Phys. Rev. Lett. **80**, 2630 (1998).
[44] J. Bosse, Nuovo Cimento A **12**, 481 (1990).